

A Rate-Theory–Phase-Field Model of Irradiation-Induced Recrystallization in UMo Nuclear Fuels

SHENYANG HU,^{1,2} VINEET JOSHI,¹ and CURT A. LAVENDER¹

1.—Pacific Northwest National Laboratory, P. O. Box 999, Richland, WA 99352, USA. 2.—e-mail: Shenyang.hu@pnnl.gov

In this work, we developed a recrystallization model to study the effect of microstructures and radiation conditions on recrystallization kinetics in UMo fuels. The model integrates the rate theory of intragranular gas bubble and interstitial loop evolutions and a phase-field model of recrystallization zone evolution. A first passage method is employed to describe one-dimensional diffusion of interstitials with a diffusivity value several orders of magnitude larger than that of fission gas xenons. With the model, the effect of grain sizes on recrystallization kinetics is simulated. The results show that (1) recrystallization in large grains starts earlier than that in small grains, (2) the recrystallization kinetics (recrystallization volume fraction) decrease as the grain size increases, (3) the predicted recrystallization kinetics are consistent with the experimental results, and (4) the recrystallization kinetics can be described by the modified Avrami equation, but the parameters of the Avrami equation strongly depend on the grain size.

INTRODUCTION

Irradiation-induced recrystallization is a general phenomenon that is often observed in nuclear fuels such as UO₂ and U-xMo dispersion and monolithic fuels.^{1–5} The recrystallization process results in submicron size grains that increase the grain boundary area per unit volume, shorten the diffusion distance of fission gas atoms and radiation defects, and destabilize intragranular gas bubbles inside recrystallized grains. As a result, it accelerates intergranular gas bubble growth rate and swelling kinetics.^{1,6} Several types of materials processes, such as casting, mechanical rolling and thermal treatment, and hot isostatic pressure are used in fuel fabrication.^{7,8} The resulting microstructural features, such as grain size, porosity, and second-phase morphology, strongly depend on the material processes and process parameters. Therefore, a fundamental understanding how microstructures produced during fuel fabrication and irradiation conditions affect recrystallization and swelling kinetics is critical for optimizing material processes to obtain desired microstructures and fuel performance.

Experiments have revealed that (1) recrystallization primarily starts on grain boundaries (and/or free surfaces), and then the recrystallization front moves toward the grain center eventually consuming the entire grain,^{1–5,9–15} and (2) recrystallization occurs at locations with a high dislocation density.^{3,9} In irradiated nuclear fuels, the cascades of high-energy fission fragments continuously generate defects. Grain boundaries are strong sinks for these irradiation-generated defects. An accumulation of interstitials at grain boundaries may lead to interstitial loop nucleation and growth. In addition, over-pressured inter- and intragranular gas bubbles might emit dislocations.^{14,16–18} Therefore, it is reasonable to assume that the recrystallization is driven by the deformation energy associated with the accumulation of dislocations and interstitial loops on grain boundaries.

A rate theory model has been extensively used to study defect evolution and recrystallization kinetics in irradiated nuclear fuels.^{11,13,15} Analytical expressions of the critical fission density at which irradiation-induced recrystallization occurs, and recrystallization kinetics in terms of critical fission density for recrystallization initiation, fission

density, and recrystallized grain size were derived. Nevertheless, the rate theory models cannot consider the effect of heterogeneous microstructures (such as grain morphology) and the evolving microstructure (such as dislocation loop distribution) on recrystallization initiation and recrystallization kinetics because all the variables of defect concentrations and size distributions were assumed to be spatially independent.

In this work, a recrystallization model in irradiated UMo fuels was developed by integrating spatially dependent rate theory and a phase-field approach.^{19,20} The rate theory model, which was developed in our previous work to study the effect of heterogeneous microstructures and inhomogeneous thermodynamic properties of defects on fission gas diffusion, intra- and intergranular gas bubble evolution, and swelling kinetics prior to recrystallization,²¹ was extended to take into account the interstitial and interstitial loop evolutions. With the assumption that the coarse grain becomes unstable when the local dislocation loop density is larger than a critical value, a phase-field model was developed to describe the transition from coarse grains to recrystallized grains. An integration of these two models enables us to study the effect of initial microstructures on dislocation loop density evolution, recrystallization initiation, and recrystallization kinetics.

MICROSTRUCTURE EVOLUTION MODELS IN POLYCRYSTALLINE UMo FUELS UNDER IRRADIATION

We consider a polycrystalline UMo fuel. The fission reaction and high-energy fission fragment cascade continuously produce Xe gas atoms and defects such as interstitials, vacancies, and their clusters. Migration, recombination, and aggregation of these defects result in the formation of intra- and intergranular gas bubbles and interstitial loops that cause volumetric swelling. The gas bubble and interstitial loops might cause lattice distortion that leads to recrystallization or grain refinement. In turn, recrystallization may affect the evolution of intra- and intergranular gas bubbles and, hence, the gas bubble swelling kinetics. In this section, we describe the thermodynamic and kinetic models of microstructure evolution, including gas bubbles, interstitial loops, and recrystallization zone.

Evolution of Intra- and Intergranular Gas Bubbles

Gas bubbles inside large grains often form a face-centered cubic (fcc) superlattice while the gas bubble superlattice structure is unstable inside small grains.^{4,5} Therefore, grain size, grain aspect ratio, and structural defects might result in a heterogeneous gas bubble structure that affects gas bubble swelling kinetics. A set of variables—fission gas Xe concentration, $c(\mathbf{r},t)$; interstitial

concentration, $c_{\text{int}}(\mathbf{r},t)$; intragranular gas bubble density, $c_b(\mathbf{r},t)$; intragranular gas bubble radius, $r_b(\mathbf{r},t)$; fission gas content per gas bubble, $n_b(\mathbf{r},t)$; and interstitial loop density—are used to describe the defect microstructure in irradiated UMo fuels. Unlike traditional rate theory, all field variables are assumed to be space- and time-dependent functions so the effect of the heterogeneous microstructure on microstructure evolution can be studied. The driving force of fission gas diffusion is generalized to be the local chemical potential gradient. Thus, the effect of local stress fields and structural defects such as grain boundaries on diffusion driving force could be naturally taken into account.^{22,23} The evolution equations of Xe concentration, intra- and intergranular gas bubbles, have been described in the supplementary data file.

Evolution of Interstitials and Interstitial Loop Density

For interstitials and interstitial loop evolution, the following assumptions have been made to simplify the problem while retaining the physics. Because intragranular gas bubbles have a high density and internal pressure, the bubbles will be strong sinks for vacancies. It is speculated that radiation-generated vacancies are quickly eliminated in the matrix via annihilation between interstitials and vacancies and the absorption by overpressured and dense intragranular gas bubbles. Therefore, the vacancy concentration is assumed to be zero in the matrix. Nevertheless, the radiation and defect reactions produce a net generation of interstitials in the matrix. The net interstitial generation rate should be equal to the vacancy absorption rate by evolving intragranular gas bubbles and can be calculated by $\dot{g}_{\text{Int}}(\mathbf{r},t) = g_0 \frac{d(c_b(\mathbf{r},t)n_b(\mathbf{r},t))}{dt}$, where g_0 is the ratio of gas atom volume inside the intragranular gas bubble and average atom volume (vacancy volume) of UMo alloys. For instance, if one gas atom occupies two vacancy sites, the ratio $g_0 = 2.0$. It is assumed that the interstitial loops are unstable in the matrix because of the compressive stress caused by the presence of overpressured gas bubbles. For simplicity, generated interstitials are distributed throughout the entire polycrystalline structure while the effect of intragranular gas bubble occupation on interstitial migration is ignored. Molecular dynamics simulations showed that emitted dislocations from the gas bubbles are captured by neighboring gas bubbles so the interstitials are assumed to exist in the most stable form, i.e., the [110] dumbbell according to density functional theory calculations.¹⁸ The interstitial usually is much more mobile than the fission gas atom Xe. It is further assumed that the interstitial migrates along the $\langle 110 \rangle$ direction in body-centered cubic (bcc) UMo alloys. Dislocations and grain boundaries are sinks for interstitials. Nucleation and growth of interstitial

loops result from accumulations of interstitials near grain boundaries that diffuse from interior grains and/or are emitted by the intergranular gas bubbles. We assumed that the nucleus density of interstitial loops near grain boundaries is constant.

Rate theory is used to describe the evolution of interstitials and interstitial loops. Interstitial concentration $c_{\text{int}}(\mathbf{r}, t)$ and interstitial loop density $\rho_{\text{loop}}(\mathbf{r}, t)$ are used to describe the spatial distribution of defects. With these assumptions, the evolution of interstitials can be described by:

$$\frac{\partial c_{\text{int}}(\mathbf{r}, t)}{\partial t} = \nabla D_{\text{int}} \nabla c_{\text{int}} + \dot{g}_{\text{int}}(\mathbf{r}, t) - D_{\text{int}} Z_{\text{iI1}} \rho_{\text{loop}}(\mathbf{r}, t) c_{\text{int}}(\mathbf{r}, t) - D_{\text{int}} Z_{\text{iI2}} \rho_{\text{dislocation}} c_{\text{int}}(\mathbf{r}, t) \quad (1)$$

where D_{int} is the diffusivity of interstitials, $\dot{g}_{\text{int}}(\mathbf{r}, t)$ is the generation rate of interstitials, $\rho_{\text{loop}}(\mathbf{r}, t)$ is the density of interstitial loops, $\rho_{\text{dislocation}}$ is the dislocation density, and Z_{iI1} and Z_{iI2} are sink coefficients of interstitials at interstitial loops and dislocations, respectively. The evolution of interstitial loops for constant density of interstitial loop nuclei can be described by the following equation²⁴:

$$\frac{\partial \rho_{\text{loop}}(\mathbf{r}, t)}{\partial t} = \frac{2\pi D_{\text{int}} Z_{\text{iI1}} N c_{\text{int}}(\mathbf{r}, t)}{|\mathbf{b}|} \quad (2)$$

where N is the density of interstitial loop nucleus at \mathbf{r} and \mathbf{b} is the Burgers vector of the interstitial loop.

By solving the evolution equations of defects, Xe atom concentration, the intragranular gas bubble morphology, the average flux of Xe atoms to grain boundaries, interstitial concentration, and interstitial loop density can be obtained. The time step solving the diffusion equations of interstitials and Xe atoms can be estimated by $\Delta t = \min(\Delta x^2/D_{\text{int}}, \Delta x^2/D_g)$, where Δx is the simulation cell grid size. It is believed that the diffusion rate the interstitials is usually several orders of magnitude faster than the diffusion rate of Xe atoms. Therefore, the interstitial diffusivity will determine the time step in the simulations. A very small time step is required to solve the diffusion equations because of the large diffusivity of interstitials, which significantly affects the numerical efficiency in simulations. In addition, the one-dimensional (1D) diffusion of interstitials along [110] direction in bcc UMo alloys and the huge difference between interstitial and Xe diffusivity increases the difficulty of solving the diffusion (Eq. 1). In this work, the 1D migration of interstitials is viewed as a random walk along specific directions. The first passage method²⁵⁻²⁷ is used to solve Eq. 1 (see the supplementary data file). Thus, large time steps determined by the Xe diffusivity can be used to enhance the numerical efficiency.

Evolution of Recrystallization Zone

A phase-field model of radiation-induced recrystallization has been developed.²⁸ The model assumes that the dislocation density is uniform in

the polycrystalline structure; recrystallization grains nucleate on grain boundaries; and the dislocation density and nucleation rate and critical grain shape are determined by the fission rate. In this work, we proposed a phase-field model of recrystallization with spatial evolution of dislocation loop density. The following assumptions were used in the model: (1) recrystallization from coarse grains to fine grains is viewed as a second-order phase transition at locations where interstitial loop density or lattice distortion is larger than a critical value; (2) the recrystallized grains have uniform radius R_{rx} ; (3) fine-grained material inside the recrystallization zone is treated as a new phase; (4) recrystallization creates a new interface between the recrystallization zone and coarse grains where the interstitial loop accumulates with the increase of fission density; and (5) recrystallization kinetics are determined by the propagation of the interface between the recrystallization zone and coarse grains. Only one order parameter $\eta(\mathbf{r}, t)$ is needed to describe the coarse grains and the recrystallization zone, which makes the simulation numerically efficient. With these assumptions, the evolution of the recrystallization zone can be described by:

$$\frac{\partial \eta(\mathbf{r}, t)}{\partial t} = -L \frac{\delta G(\eta, \rho_{\text{loop}})}{\delta \eta} \quad (3)$$

where $G(\mathbf{r}, t)$ is the total free energy of the system and κ is the gradient energy coefficient. The total free energy is calculated by:

$$G(\eta, \rho_{\text{loop}}) = \int_V [f(\eta, \rho_{\text{loop}}) + \frac{\kappa}{2} |\nabla \eta|^2] dV \quad (4)$$

where $f(\eta, \rho_{\text{loop}})$ is the free energy density. For the transition from coarse grains to recrystallized grains, the following free energy density is used:

$$f = 4\eta^2(1 - \eta)^2 - \rho_0^* \frac{15}{4} \left(\eta - \frac{2}{3}\eta^3 + 0.2\eta^5 \right) \quad (5)$$

$$\rho_0^* = \frac{0.3}{\exp\left(-20\left(\frac{\rho_{\text{loop}}}{\rho_{\text{crit}}} - 0.7\right) + 1.0\right)} \quad (6)$$

where ρ_{crit} is the critical interstitial loop density. Atomistic simulations showed that the pressured intragranular gas bubbles continuously emit dislocations.¹⁸ The dislocation density inside the coarse grain increases as the fission density increases. Therefore, ρ_{crit} should decrease as the fission density increases. In this work, the fission density dependence of critical interstitial loop density is expressed by $\rho_{\text{crit}} = \rho_{\text{crit}}^0 + \Delta\rho_{\text{crit}}^0 / \exp\left(-20\left(\frac{\text{FD}}{\text{FD}_{\text{crit}}} - 0.7\right) + 1.0\right)$, where FD is the fission density, FD_{crit} is the critical fission density, and $\Delta\rho_{\text{crit}}^0$ is the critical density of dislocations associated with the accumulation of emitted dislocations from gas bubbles. The free energy function f is plotted (see Fig. S2 in the

supplementary file). The free energy indicates that (1) the coarse grain phase and recrystallized grain phase coexist when the interstitial loop density is small ($\rho_0^* < 0.5$), and (2) the matrix phase becomes unstable when the interstitial loop density approaches the critical value of interstitial loop density. Therefore, recrystallized grains form where the dislocation loop density is larger than the critical value. The introduction of nuclei, which is often needed in previous phase-field models,^{22,28–32} is not necessary in the simulations.

Integrating Eqs. S1 to S8 and 1 to 3, we have the microstructure-dependent, rate-theory–phase-field model of irradiation-induced recrystallization in UMo alloys. In the simulations, total Xe atoms inside the matrix of coarse grains, intra- and intergranular gas bubbles, and recrystallization zone increases as the fission density increases, and satisfy the mass conservation. The intragranular gas bubble is assumed to be unstable once the recrystallization zone front sweeps coarse grains. Xe atoms inside the intragranular gas bubbles dissolve and diffuse to the gas bubbles inside the recrystallization zone. The gas bubble evolution inside the recrystallization zone was not considered in this work. But the development of gas bubble evolution model is under way.

RESULTS AND DISCUSSION

The initial polycrystalline structures used in the simulations are created by a phase-field model of grain growth.³³ The phase-field modeling outputs the order parameters that describe the grain orientations. The order parameter fields $y_i(\mathbf{r})$, ($i = 1, 2, \dots, m$), which is 1.0 inside grain i and 0.0 outside grain i and varies smoothly from 1.0 to zero across the grain boundaries, are used to set up the initial structure. A variable $\eta_0(\mathbf{r}, t)$ is defined to describe the grain boundary region, which is defined as:

$$\eta_0(\mathbf{r}, t)|_{t=0} = \sum_{i=1}^m [1 - y_i(\mathbf{r})]^2 \quad (7)$$

The value of $\eta_0(\mathbf{r}, t)$ is zero inside the grains and larger than zero inside the grain boundary region where interstitial loops nucleate and grow. For the phase-field model of recrystallization, the initial value of the order parameter $\eta(\mathbf{r}, t)$, which describes the coarse grains and recrystallization zone, is set to zero (i.e., the initial structure only consists of coarse grains). The value of $\eta(\mathbf{r}, t)$ becomes 1 when the local interstitial loop density is larger than the critical value. Then, the grain boundaries include the initial coarse grain boundaries and the interface between the recrystallization zone and the coarse grains. The grain boundary region $\eta_0(\mathbf{r}, t)$ is updated by:

$$\eta_0(\mathbf{r}, t) = \begin{cases} \sum_{i=1}^m [1 - y_i(\mathbf{r})]^2, & \text{if } \eta(\mathbf{r}, t) = 0.0 \\ \sum_{i=1}^m [1 - (y_i(\mathbf{r}) - \eta(\mathbf{r}, t))]^2 + (1 - \eta(\mathbf{r}, t))^2, & \text{if } \eta(\mathbf{r}, t) > 0.0 \end{cases} \quad (8)$$

In the simulation, the nucleus density of interstitial loops is assumed to be a constant of N when $\eta_0(\mathbf{r}, t) > 0$ (i.e., inside the grain boundaries). Prior to recrystallization, the evolution of both intra- and intergranular gas bubbles are simulated. Once the recrystallization takes place, only intragranular gas bubble evolution is considered because there is no gas bubble evolution model available inside the recrystallization zone. But the total Xe atoms inside the recrystallization zone are calculated, which includes Xe atoms in intergranular gas bubbles, Xe atoms generated by U fission, and the dissolved Xe atoms when the recrystallization zone front sweeps the intragranular gas bubbles. The Xe atom accumulation can be used to simulate the gas bubble evolution and swelling inside the recrystallization zone in future. The model parameters are listed in Table SI in the supplementary data file. All the model parameters on defect evolution are chosen by assessing the parameters used in the rate theory models.^{1,13,15} This phase-field model describes the phase stability, while the recrystallization kinetics are controlled by interstitial loop accumulation kinetics. Therefore, phase-field model parameters such as interface mobility and interfacial energy can be chosen to ensure numerical convergence and efficiency. It should be pointed out that the model parameters (critical densities of interstitial loops, dislocations, and fission density) of free energy functions in Eqs. 5 and 6 are not well known because of the lack of experimental data. In addition, the value of a gradient coefficient may affect the recrystallization kinetics at the earlier recrystallization stage that is discussed in the supplementary data file.

Recrystallization Kinetics in Bi-Crystalline Structures

First we consider irradiation-induced recrystallization in a bi-crystalline structure with different grain sizes. The simulation cell has dimensions of $n_x l_0 \times n_y l_0 \times n_z l_0$. The terms n_x , n_y , and n_z are grid numbers in the x , y , and z directions, respectively. Periodic boundary conditions are applied in three directions. Grain 1 is placed at the center of the simulation cell, while grain 2 is placed at both ends of the simulation cell to satisfy the periodic boundary condition in the x direction. The two grains have the same diameter of $n_x l_0 / 2$. The values of n_y and n_z are set to 4 and 8, respectively. The values of n_x are

set to be 128, 256, 512, 1024, 2048, and 4096 to study the effect of grain sizes on recrystallization kinetics. In the simulations, the diffusivity of the interstitials is five orders of magnitude larger than the diffusivity of Xe. Such a setup of simulation conditions degenerate the problem to a one-dimensional (1D) problem.

Two parameters are used to describe the recrystallization kinetics. One is the normalized thickness of recrystallization zone, which is defined as:

$$H_{\text{Rx}}^* = \frac{V_{\text{Rx}}}{V_{\text{GB}}} \quad (9)$$

where V_{GB} is the volume of grain boundaries at zero fission density ($V_{\text{GB}} = 2S_{\text{GB}} \times l_0$, S_{GB} is the total area of the grain boundaries), and V_{Rx} is the volume of recrystallization zone at a given fission density. For bi-crystalline structures, H_{Rx}^* actually defines the recrystallization zone thickness normalized by the grain boundary thickness. For polycrystalline structures, H_{Rx}^* presents an effective recrystallization zone thickness because the radius of coarse grains change with time. Another parameter is the volume fraction of the recrystallization zone that is commonly used and defined as:

$$V_{\text{Rx}}^* = \frac{V_{\text{Rx}}}{V_0} \quad (10)$$

where V_0 is the volume of the simulation cell ($V_0 = n_x \times n_y \times n_z l_0^3$).

The effect of grain sizes on H_{Rx}^* and V_{Rx}^* is plotted in Fig. 1. Figure 1a clearly illustrates the tendency of the growth rate H_{Rx}^* , with respect to the fission density, to increase as the grain size increases. The growth rate H_{Rx}^* approaches a constant with the grain size increase. This kinetic phenomenon can be explained by the net interstitial concentration inside the grains and the interstitial mobility. A large grain has more interstitials available, which speeds up the formation and accumulation of interstitial loops at grain boundaries and, hence, the recrystallization kinetics. On the other hand, the interstitial diffusivity also affects the interstitial accumulation kinetics at the grain boundary. The diffusion distance of interstitials can be estimated by $\sqrt{D_{\text{int}}\Delta t}$. This implies that if the grain radius is larger than $\sqrt{D_{\text{int}}\Delta t}$, the interstitials inside the central region of grains could not reach the grain boundary during the time increment Δt . As a consequence, grains with radii larger than a critical radius depending on D_{int} should have the same growth rate of H_{Rx}^* as shown in Fig. 1a. An opposite tendency is observed in Fig. 1b; that is, the recrystallization kinetic rate V_{Rx}^* decreases as the grain size increases. This finding is consistent with the growth rate of H_{Rx}^* .

Recrystallization Kinetics in Two-Dimensional (2D) Polycrystalline Structures

With the same model parameters and radiation conditions, we simulated the effect of grain sizes on recrystallization kinetics in polycrystalline structures. The simulation cell has dimensions of $n_x l_0 \times 4l_0 \times n_x l_0$. Three initial grain structures with different average grain diameters $D = 1.34 \mu\text{m}$, $4.36 \mu\text{m}$, and $8.72 \mu\text{m}$ were generated in simulation cells with $n_x = 200$, 200 , and 400 by the phase-field model of grain growth. The grain structure is identical along the y direction so it is a 2D problem. The grain boundary in the rate-theory-phase-field model of recrystallization kinetics is treated as a sharp interface. In other words, the grain boundary thickness is zero. So the polycrystalline structure with diffusive grain boundaries obtained from the phase-field simulation of grain growth is converted to have sharp grain boundaries before recrystallization modeling. In the simulations, the interstitials diffuse along $\langle 101 \rangle$ directions with $D^* = 1.0 \times 10^5$, while Xe diffuses isotopically. Figure 2 shows the time evolution of the intragranular gas bubble density in a polycrystalline structure with an average grain diameter of $4.36 \mu\text{m}$. The blue regions are grain boundaries and the evolving recrystallization zone, which starts at the grain boundaries and propagates to the center of grains. Some features on the evolution of the gas bubble density were observed: (1) gas bubble density increases as fission density increases, (2) gas bubble density is not uniform (i.e., it is higher at the grain center than near grain boundaries) and higher inside large grains than that inside small grains, and (3) recrystallization in small grains completes earlier than that in large grains. The temporal evolution of the interstitial loop density, intra-granular gas bubble density, Xe content per gas bubble, and gas bubble radius on the line A–A' shown in Fig. 2a are plotted in Fig. S4 in the supplementary data files.

Figure 3 shows the effect of average grain sizes on intragranular gas bubble structures at fission density of 2.25×10^{27} fissions/ m^3 . The average grain sizes in Fig. 3a, b, and c are $1.34 \mu\text{m}$, $4.36 \mu\text{m}$, and $8.72 \mu\text{m}$, respectively. Since the same color bar is used for different grain structures, it can be clearly seen that intragranular gas bubble structures strongly depend on the average grain size. As the average grain size increases, the gas bubble density, Xe content per bubble and gas bubble radius increases. The effects of average grain sizes on recrystallization kinetics are shown in Fig. S3 in the supplementary data file. The fission density dependence of H_{Rx}^* and V_{Rx}^* is the same as that shown in Fig. 1 for bi-crystalline and polycrystalline structures. The results confirm the conclusions that (1) the growth rate of H_{Rx}^* increases as the grain size increases and (2) the recrystallization kinetic rate

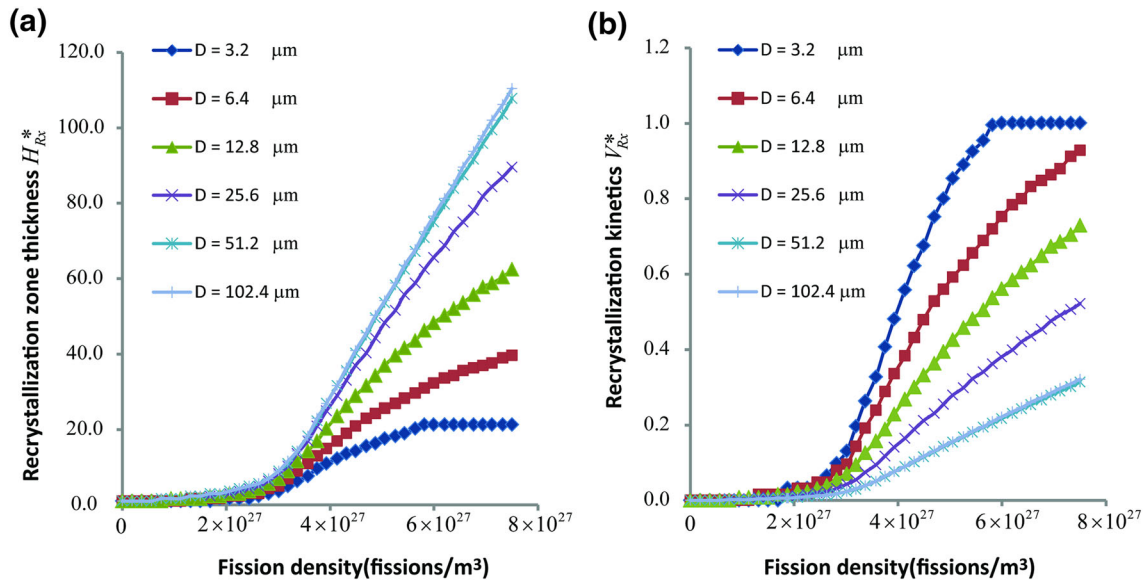


Fig. 1. Effect of grain sizes on recrystallization kinetics: (a) recrystallization zone thickness and (b) recrystallization kinetics.

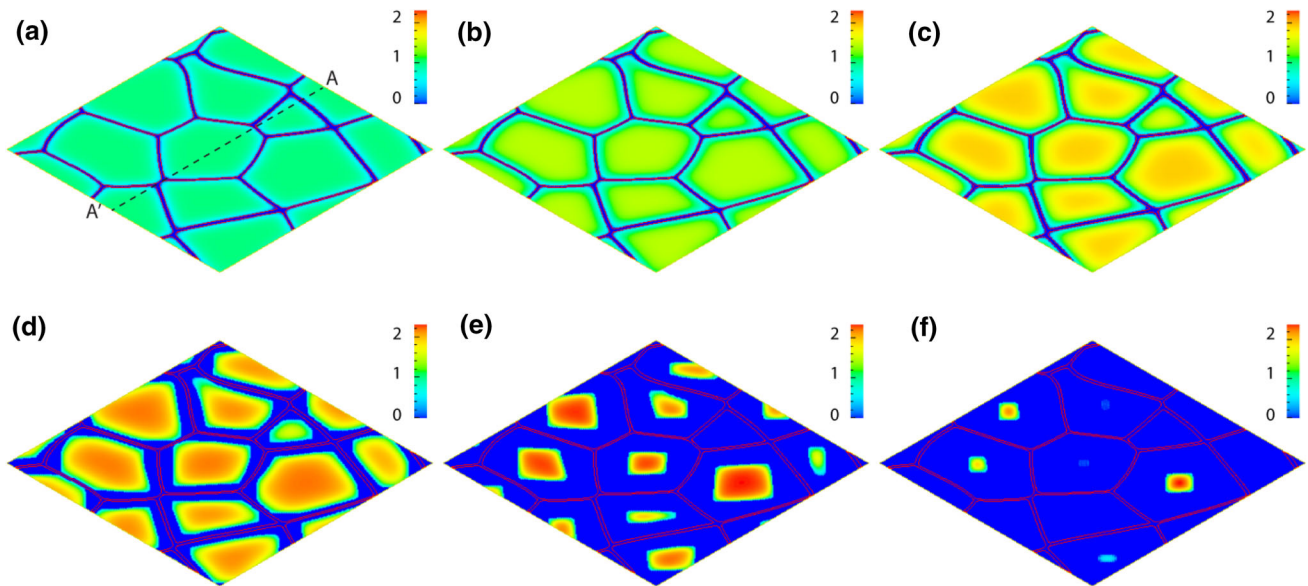


Fig. 2. Snapshots of the intragranular gas bubble density distribution on the central plane ($y = 2l_0$) of the simulation cell $200l_0 \times 4l_0 \times 200l_0$ at different fission densities (a) 1.87×10^{26} , (b) 7.5×10^{26} , (c) 2.25×10^{27} , (d) 3.01×10^{27} , (e) 5.05×10^{27} , and (f) 7.5×10^{27} fissions/ m^3 in a polycrystalline structure with an average grain diameter of $4.36 \mu m$ under a fission rate of 8.2×10^{20} fissions/ m^3s . The color bar denotes the gas bubble density in units of $10^{24}/m^3$.

V_{Rx}^* decreases as the grain size increases. All of these results are consistent with experimental observations.⁴

Discussion

The recrystallization kinetics are described by a modified Avrami equation as follows^{34,35}:

$$V_{Rx}^* = 1 - \exp(-k(FD - FD_0)^n) \quad (11)$$

where k is the recrystallization reaction constant and FD is the fission density (10^{27} fissions/ m^3). FD_0 is the incubation fission density above which recrystallization occurs, and n is the Avrami exponent that depends on nucleation and growth mechanisms. Kim et al.¹ developed an empirical formula of recrystallization kinetics with experimental data for UMo fuel under fission rates in the $2.4\text{--}6.8 \times 10^{20}$ fissions/ m^3s range. One set of the parameters for k , FD_0 , and n in Eq. 11 was suggested as

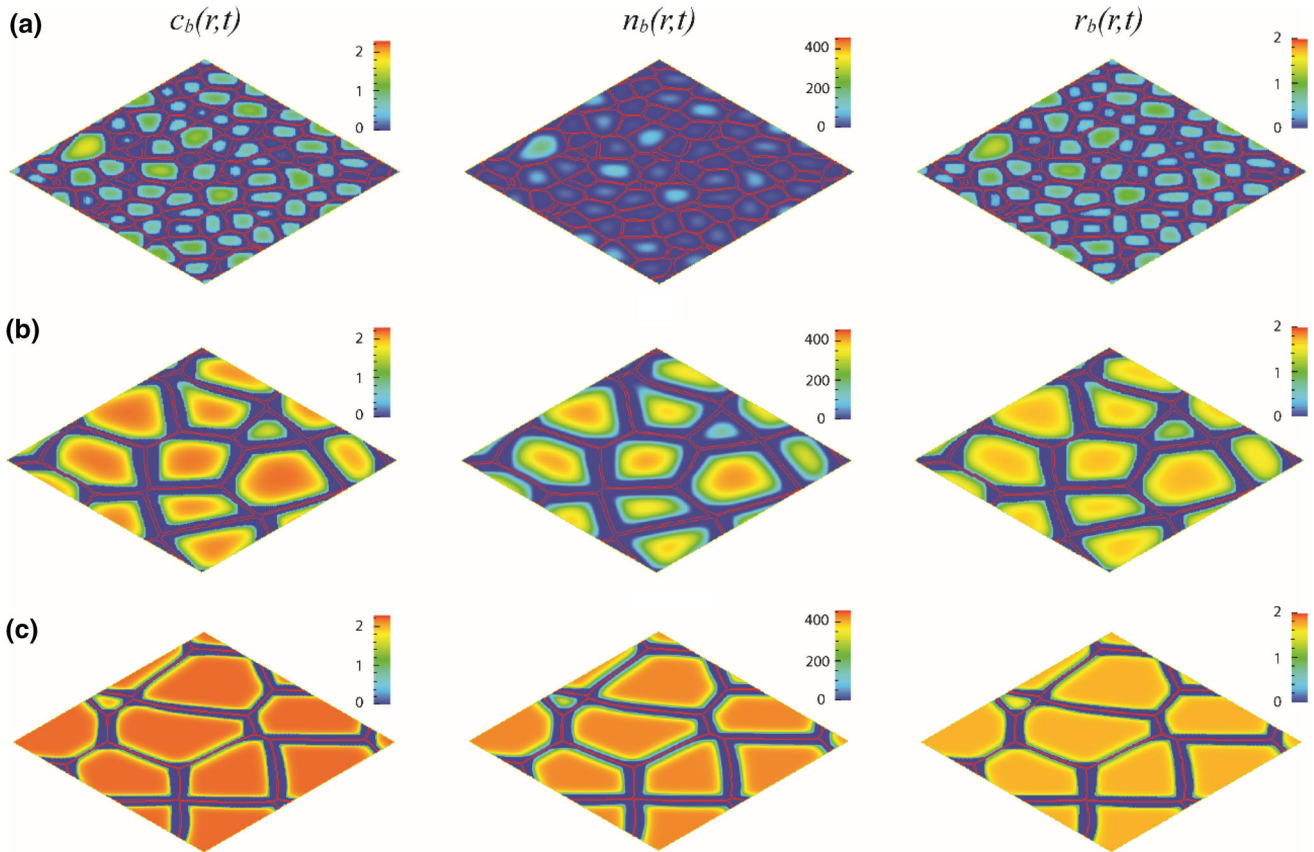


Fig. 3. Effect of average grain sizes on intragranular gas bubble microstructures at a fission density of 2.25×10^{27} fissions/m³ under a fission rate of 8.2×10^{20} fissions/m³s. Average grain sizes: (a) 1.34 μm , (b) 4.36 μm , and (c) 8.72 μm . The color bars for gas bubble density $c_b(r,t)$, Xe content $n_b(r,t)$, and gas bubble radius $r_b(r,t)$ have the units of $10^{24}/\text{m}^3$, Xe atom numbers per bubble, and nm, respectively.

$k = 0.1 \times [0.75(10 - c_{\text{Mo}}) + 1]$, where c_{Mo} is the Mo content in wt.%; $\text{FD}_0 = 1.67$ for atomized powder fuel; and $n = 2.6$. Figure 4 presents the recrystallization kinetics obtained from experiments, theoretical models (empirical formula)¹ and simulations. Simulation results in 1D (bi-crystalline) and 2D (polycrystalline) grain structures show that the recrystallization kinetics decrease as the grain size increases from 1.34 μm , 3.20 μm , 4.36 μm , and 6.40 μm . We found that the predicted recrystallization kinetics for grain sizes from 3.2 μm to 6.4 μm falls into the region of experimental points if experimental error is taken into account. Noting that the average grain size in experimental samples is about 4–5 μm ,³⁶ we concluded that the recrystallization kinetics predicted from simulations is consistent with experimental results.¹ The results calculated by the empirical formula of Eq. 11 agree well with the recrystallization kinetics predicted by the simulations for the fuel with a grain diameter of 3.2 μm . It also indicates that the recrystallization kinetics can be described by the modified Avrami equation. Nevertheless, the strong grain size dependence of the recrystallization kinetics shown in Figs. 1b, 4, and Fig. S3b (see the supplementary

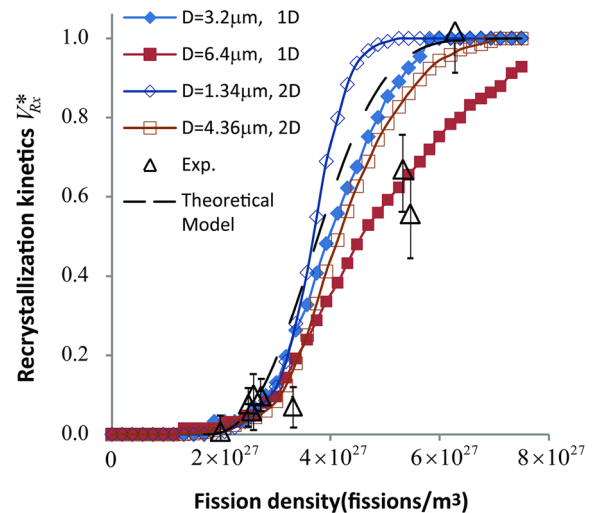


Fig. 4. Effect of average grain sizes on recrystallization kinetics.

materials) suggested that the parameters k , FD_0 , and n in Eq. 11 should strongly depend on the grain size.

Both 1D and 2D simulation results show a consistent tendency that recrystallization kinetics decrease as grain size increases. Simulations in three-dimensional (3D) polycrystalline structures, however, are desired to more quantitatively understand the effect of grain size on recrystallization kinetics. Although the first passage method greatly improved numerical efficiency in solving the diffusion equations of Xe and interstitials, a 3D simulation is still a computationally intensive process because the interstitial diffusivity is several orders of magnitude larger than the diffusivity of Xe. Therefore, a highly scalable numerical method is required for the application of the model in 3D simulations.

The developed recrystallization model combining rate theory and the phase-field method is able to obtain the intragranular gas bubble structures and Xe flux to grain boundaries as well as the recrystallization zone. Prior to recrystallization, the Xe flux to grain boundaries can be used to calculate the intergranular gas bubble structures including intergranular gas bubble density and size. Therefore, the effect of grain sizes on gas bubble swelling can be assessed.²¹ After recrystallization occurs, intergranular gas bubble evolution cannot be predicted with Eqs. S7 and S8 because the grain boundary area changes with time. Furthermore, at high fission density, the intergranular gas bubble might transfer to voids, which would greatly increase swelling kinetics.^{37–39} To evaluate the effect of grain morphology and recrystallization on gas bubble swelling, it is important to correctly describe intergranular gas bubble evolution in the recrystallization zone as well as the gas bubble-to-void transition.

CONCLUSION

In this work, we developed a rate-theory–phase-field model of recrystallization kinetics in irradiated UMo nuclear fuels. The model allows the effect of grain size on recrystallization kinetics and intragranular gas bubble microstructure evolution to be studied. The rate-theory model describes the evolution of gas bubbles, interstitials, and interstitial loops while the phase-field model describes evolution of the recrystallization zone. From 1D simulations in bi-crystalline structures and 2D simulations in polycrystalline structures, we can conclude that (1) recrystallization in large grains starts earlier than that in small grains, (2) the recrystallization kinetics (recrystallization volume fraction) decreases as the grain size increases, (3) the predicted recrystallization kinetics is consistent with the experimental results, and (4) the recrystallization kinetics can be described by the modified Avrami equation, but the parameters of the Avrami equation strongly depend on the grain size. The simulation results also showed that the gas bubble density, Xe content per gas bubble, and gas bubble

radius increase as grain size increases. The developed model can describe the evolution of intragranular gas bubble microstructures and the Xe flux to the recrystallization zone after recrystallization takes place. Nevertheless, it cannot calculate the total swelling of gas bubbles because intergranular gas bubble evolution in the recrystallization zone is not known. The model needs further development to include a capability for describing the intergranular gas bubble evolution and gas bubble-to-void transition in the recrystallization zone to predict the effect of recrystallization on swelling kinetics.

ACKNOWLEDGEMENTS

The work described in this article was performed by Pacific Northwest National Laboratory, which is operated by Battelle for the U.S. Department of Energy under Contract DE-AC05-76RL01830. This study was supported by the U.S. Department of Energy, National Nuclear Security Administration Office of Material Management and Minimization Reactor Conversion Program. Dr. Hu would like to thank Nicholas Lombardo at PNNL for the comments.

ELECTRONIC SUPPLEMENTARY MATERIAL

The online version of this article (doi:[10.1007/s11837-017-2611-4](https://doi.org/10.1007/s11837-017-2611-4)) contains supplementary material, which is available to authorized users.

REFERENCES

1. Y.S. Kim, G.L. Hofman, and J.S. Cheon, *J. Nucl. Mater.* 436, 14 (2013).
2. J. Spino, D. Baron, M. Coquerelle, and A.D. Stalios, *J. Nucl. Mater.* 256, 189 (1998).
3. K. Nogita and K. Une, *Nucl. Instrum. Methods B* 91, 301 (1994).
4. J. Gan, D.D. Keiser, B.D. Miller, A.B. Robinson, J.F. Jue, P. Medvedev, and D.M. Wachs, *J. Nucl. Mater.* 424, 43 (2012).
5. Y.S. Kim and G.L. Hofman, *J. Nucl. Mater.* 419, 291 (2011).
6. M.K. Meyer, J. Gan, J.F. Jue, D.D. Keiser, E. Perez, A. Robinson, D.M. Wachs, N. Woolstenhulme, G.L. Hofman, and Y.S. Kim, *Nucl. Eng. Technol.* 46, 169 (2014).
7. G. Moore, AFIP-2 Fabrication Summary Report (INL/EXT-08-14871, 2010).
8. D.E. Burkes, A.M. Casella, E.C. Buck, A.J. Casella, M.K. Edwards, P.J. MacFarlan, K.N. Pool, B.D. Slonecker, F.N. Smith, F.H. Steen, and R.E. Thornhill, Fuel Thermo-physical Characterization Project, Fiscal Year 2013 Final Report (PNNL-22981, 2013).
9. S. Kashibe, K. Une, and K. Nogita, *J. Nucl. Mater.* 206, 22 (1993).
10. L.E. Thomas, C.E. Beyer, and L.A. Charlot, *J. Nucl. Mater.* 188, 80 (1992).
11. M. Kinoshita, *J. Nucl. Mater.* 248, 185 (1997).
12. H. Matzke, *J. Nucl. Mater.* 189, 141 (1992).
13. J. Rest, *J. Nucl. Mater.* 326, 175 (2004).
14. C.B. Lee and Y.H. Jung, *J. Nucl. Mater.* 279, 207 (2000).
15. J. Rest, *J. Nucl. Mater.* 346, 226 (2005).

16. J. Spino, K. Vennix, and M. Coquerelle, *J. Nucl. Mater.* 231, 179 (1996).
17. M.V. Speight, *Nucl. Sci. Eng.* 37, 180 (1969).
18. S.Y. Hu, W. Setyawan, V.V. Joshi, and C.A. Lavender, *J. Nucl. Mater.* 490, 49 (2017).
19. L.Q. Chen, *Ann. Rev. Mater. Res.* 32, 113 (2002).
20. Y.L. Li, S.Y. Hu, X. Sun, and M. Stan, *NPJ Comput. Mater.* 3, 16 (2017).
21. S.Y. Hu, D. Burkes, C.A. Lavender, and V. Joshi, *J. Nucl. Mater.* 480, 323 (2016).
22. S.Y. Hu, C.H. Henager, H.L. Heinisch, M. Stan, M.I. Baskes, and S.M. Valone, *J. Nucl. Mater.* 392, 292 (2009).
23. N. Moelans, B. Blanpain, and P. Wollants, *Phys. Rev. B* 78, 024113 (2008).
24. N.M. Ghoniem and D. Walgraef, *Model. Simul. Mater. Sci. Eng.* 1, 569 (1993).
25. T. Opplestrup, V.V. Bulatov, G.H. Gilmer, M.H. Kalos, and B. Sadigh, *Phys. Rev. Lett.* 97, 230602 (2006).
26. S.Y. Hu and C.H. Henager, *J. Nucl. Mater.* 394, 155 (2009).
27. S.Y. Hu, D.E. Burkes, C.A. Lavender, D.J. Senior, W. Setyawan, and Z.J. Xu, *J. Nucl. Mater.* 479, 202 (2016).
28. L. Liang, Z.G. Mei, Y.S. Kim, B. Ye, G. Hofman, M. Anitescu, and A.M. Yacout, *Comput. Mater. Sci.* 124, 228 (2016).
29. A. El-Azab, K. Ahmed, S. Rokkam, and T. Hochrainer, *Curr. Opin. Solid State Mater. Sci.* 18, 90 (2014).
30. A.A. Semenov and C.H. Woo, *J. Nucl. Mater.* 454, 60 (2014).
31. S. Rokkam, A. El-Azab, P. Millett, and D. Wolf, *Model. Simul. Mater. Sci. Eng.* 17, 064002 (2009).
32. P.C. Millett, A. El-Azab, S. Rokkam, M. Tonks, and D. Wolf, *Comput. Mater. Sci.* 50, 949 (2011).
33. C.E. Krill and L.Q. Chen, *Acta Mater.* 50, 3057 (2002).
34. G.L. Hofman, J. Truffert, and J.M. Dupouy, *J. Nucl. Mater.* 65, 200 (1977).
35. F.J. Humphreys and M. Hatherly, *Recrystallization and Related Annealing Phenomena*, 2nd ed. (Oxford: Elsevier, 2004).
36. S.Y. Hu, V. Vineet, C.A. Lavendar, N.J. Lombardo, J. Wight, B. Ye, Z.G. Mei, L. Liang, M.Y. Abdellatif, G. Hofman, Y.F. Zhang, B. Beeler, X.M. Bai, J. Cole, and B. Rabin, *Microstructural Level Fuel Performance Modeling of UMo Monolithic Fuel* (Idaho Falls: Idaho National Laboratory, 2016).
37. A. Hishinuma and L.K. Mansur, *J. Nucl. Mater.* 118, 91 (1983).
38. J. Rest, *J. Nucl. Mater.* 207, 192 (1993).
39. V.I. Dubinko, *J. Nucl. Mater.* 206, 1 (1993).